MNE 17 (2022) 100167

Contents lists available at ScienceDirect

Micro and Nano Engineering

journal homepage: www.sciencedirect.com/journal/micro-and-nano-engineering

Gain and lasing from CdSe/CdS nanoplatelet stripe waveguides

Martin Belitsch [a], Dmitry N. Dirin [b,c], Maksym V. Kovalenko [b,c], Kevin Pichler [d], Stefan Rotter [d], Ahmed Ghalgaoui [e], Harald Ditlbacher [a], Andreas Hohenau [a], Joachim R. Krenn [a,*]

[a] Institute of Physics, University of Graz, 8010 Graz, Austria
[b] Institute of Inorganic Chemistry, Department of Chemistry and Applied Biosciences, ETH, 8093 Zürich, Switzerland
[c] Empa - Swiss Federal Laboratories for Materials Science and Technology, Laboratory for Thin Films and Photovoltaics, 8600 Dübendorf, Switzerland
[d] Institute for Theoretical Physics, TU Wien, 1040 Vienna, Austria
[e] Max-Born-Institut für Nichtlineare Optik und Kurzzeitspektroskopie, 12489 Berlin, Germany

ARTICLE INFO

Keywords:
Quantum dots
Nanoplatelets
Lasing

ABSTRACT

Colloidal semiconducting nanocrystals are efficient, stable and spectrally tunable emitters, but achievable optical gain is often limited by fast nonradiative processes. These processes are strongly suppressed in slab-shaped nanocrystals (nanoplatelets), due to relaxed exciton Coulomb interaction. Here, we show that CdSe/CdS nanoplatelets can be engineered into (sub)microscopic stripe waveguides that achieve lasing without further components for feedback, i.e., just relying on the stripe end reflection. We find a remarkably high gain factor for the CdSe/CdS nanoplatelets of 1630 cm^{-1}. In addition, by comparison with numerical simulations we assign a distinct emission peak broadening above laser threshold to emission pulse shortening. Our results illustrate the feasibility of geometrically simple monolithic microscale nanoplatelet lasers as an attractive option for a variety of photonic applications.

1. Introduction

Colloidal quantum dots (QDs) are semiconductor nanoparticles with high photoluminescence (PL) quantum yield, tunable optical properties, photostability and solution processability. These properties make them attractive candidates for laser gain media. For optical gain, more than one exciton per QD is needed on average, as two charge carriers with opposite spin populate the band edge levels. However, the biexciton is depopulated quickly by nonradiative Auger recombination, typically in the order of a few tens of ps [1]. Therefore, only moderate gain is typically available from QDs, mostly for pulsed excitation with rather high energy densities [1]. To suppress the Auger rate, various approaches have been implemented, such as nanorod and tetrapod geometries or specific giant shells. For example, graded shell QDs [2–4] have even enabled electrically pumped gain [5]. Another approach to mitigate Auger recombination is to spectrally separate QD absorption and emission [6]. Recently, with colloidal nanoplatelets (NPLs, "colloidal quantum wells") another particularly efficient QD species has been introduced. NPLs resemble slabs with a lateral size of about 10 − 30 nm and with a well-controlled thickness of a few atom layers [7]. Due to a relaxed exciton localization in the laterally extented slab geometry, as compared to spherical QDs, significantly reduced Auger rates were achieved [7–9]. With NPLs, amplified spontaneous emission (ASE) with pump thresholds as low as 3 $\mu J/cm^{-2}$ has been achieved [10,11] and a threshold of 6 $\mu J/cm^{-2}$ was reported to enable cw-operation [12]. NPLs also provide optical gain values significantly higher than conventional QDs [8,13,14], up to a recently reported value of 6600 cm^{-1} [15]. Generally, the high gain enabled lasing at different NPL-geometry-dependent wavelengths [16], in cw mode [12,17] and under 2- and 3-photon excitation [18]. A variety of configurations was demonstrated [19], including resonators with in-plane reflectors built solely from NPLs [20].

In this Letter, we apply CdSe/CdS NPLs as the building material of lithographically tailored stripe waveguides 500 nm and 1 μm wide. On this platform, we investigate spontaneous emission, ASE and lasing. Lasing is relying on stripe end face reflection, i.e., operating without external mirrors, an approach that renders structure fabrication simple and scalable. We retrieve laser thresholds for pump fluences of 50 − 200 $\mu J/cm^2$ for stripe lengths between 60 − 20 μm. We measure a modal gain of 1630 cm^{-1}, which is well within the highest values reported so far [8,14,15]. Furthermore, a broadening of the emission peak above treshold for increasing pump intensities is observed, which, based

* Corresponding author.
E-mail address: joachim.krenn@uni-graz.at (J.R. Krenn).

https://doi.org/10.1016/j.mne.2022.100167
Received 31 May 2022; Received in revised form 30 September 2022; Accepted 15 October 2022
Available online 19 October 2022

on numerical simulations, we assign to pulse shortening.

2. Experimental

Our colloidal CdSe/CdS NPLs consist of an atomically flat NPL CdSe core sandwiched between CdS layers. The 1.2 nm thick CdSe core consists of four complete CdSe monolayers with an additional layer of Cd atoms (so that both sides are Cd-terminated), with lateral dimensions of approximately 20 × 7 nm^2 [21,22]. A CdS shell three monolayers thick has been grown on each side of the core by colloidal atomic layer deposition, similar to a method reported earlier [8] (see Methods).

Optical spectra of CdSe/CdS NPLs in hexane solution are shown in Fig. 1a. The absorbance (blue) is dominated by two prominent peaks corresponding to the heavy and light hole transitions [9]. The PL spectrum (red), shows an emission maximum at 620 nm and a full-width-at-half-maximum (fwhm) spectral width of about 25 nm [23].

The fabrication scheme of the NPL stripe waveguides is sketched in Fig. 1b. Electron beam lithography (EBL) was used to transfer the stripe pattern to a polymer resist thin film on a glass substrate, followed by chemical development, the deposition of the NPLs by spin-coating (resulting in presumably random nanoplatelet orientation) and resist lift-off (see Methods). We fabricated NPL stripes with either a width of 500 nm and a height of 200 nm or a width of 1 μm and a height of 150 nm. The stripe length was varied from 20 − 80 μm in steps of 10 μm, see the scanning electron microscope (SEM) image of three stripes in Fig. 1c. We note that the upper edges of the nominally rectangular cross section of the stripe are somewhat elevated, most likely due to adhesion forces in the resist mask during spin coating. These edges play, however, no important role for the waveguide characteristics. The stripes were free from cracks and the average surface roughness was <5 nm root mean square, as measured by atomic force microscopy. By ellipsometry on extented NPL films we deduced an effective refractive index of 1.9 at a wavelength of 650 nm, indicating an estimated NPL packing density of about 64% [8].

For optical excitation, the broadband emission of a pulsed supercontinuum laser was selected in the wavelength band 450–550 nm. Laser pulse duration and repetition frequency were 6 ps and 100 kHz, respectively. The beam was shaped by an achromatic cylindrical lens, reflected from a dichroic mirror and then focused by an oil immersion objective (60×, 1.4 numerical aperture) to a line focus of 2 µm × 88 µm, where the former corresponds to the 1/e intensity of the Gauss profile and the latter gives the length of the top-head profile. The pump fluence was varied between 10 and 550 $\mu J/cm^2$. The NPL stripes were illuminated by the line focus (Fig. 1c) and the emitted light was collected by the same objective and transmitted through the dichroic mirror and a longpass filter. It was then dispersed by a monochromator and the spectrum was detected by a CCD camera. Alternatively, the sample was imaged by the CCD camera, which allowed to assess sample homogeneity and to detect defects. Furthermore, hybrid images were taken, combining one spatial axis (along the stripe axis) with the spectral information from each axis point displayed in the normal direction. As this setup enables sample imaging, we can routinely assess the overall quality of the (sub)microscale waveguides and identify possible scattering defects. We note that we used this detection geometry as well for the variable stripe length (VSL) method, to determine the effective gain, as described below. Comparing with the usual detection geometry with a microscope objective imaging the film (or waveguide) end face (i.e., being oriented perpendicularly to the excitation optics), we found no significant differences in the measured relative light intensities, which we assign to the large collection angle of the used objective.

3. Results and discussion

The evolution of the NPL emission from a 70 µm long stripe under increasing pump fluence is illustrated by the exemplary spectra in Fig. 2a. The pump line focus overlaid the whole stripe length. Spontaneous emission (pump fluence 84 $\mu J/cm^2$) is plotted in blue, acquired from the middle position of the stripe (blue circle in the inset sketch). For the same pump fluence the signal acquired from the stripe end (light red curve and circle) is already enhanced due to ASE that is preferentially contributing to the waveguide mode and that is then scattered at the stripe end face [8,14]. The spectral shift of the ASE peak is due to the redshifted emission of biexcitons, as compared to excitonic emission. [24,25]. For a pump fluence of 260 $\mu J/cm^2$ we observe laser emission, as plotted in the dark red spectral curve. Here, the emission intensity increases by about three orders of magnitude. As further discussed below, laser thresholds turn out to be between 50 and 200 $\mu J/cm^2$ for stripe lengths between 60 and 20 µm.

Fig. 2b depicts spectra acquired for a pump fluence of 260 $\mu J/cm^2$ at the end of stripes 20, 40 and 80 μm long. The spectral line spacing is given by the free spectral range of the longitudinal modes in the Fabry-Pérot resonator formed by the stripes, which is about 4 nm (length 20 µm), 2 nm (length 40 µm) and 1 nm (length 80 μm). Accordingly, we deduce an *effective* mode index around 1.6, which agrees well with the ellipsometry data taken on extented NPL films and thus confirms the structural homogeneity of the stripes. The mode index value is further verified by finite-difference time-domain (FDTD) simulations of the stripes (see the Supporting Information). In addition, the simulations

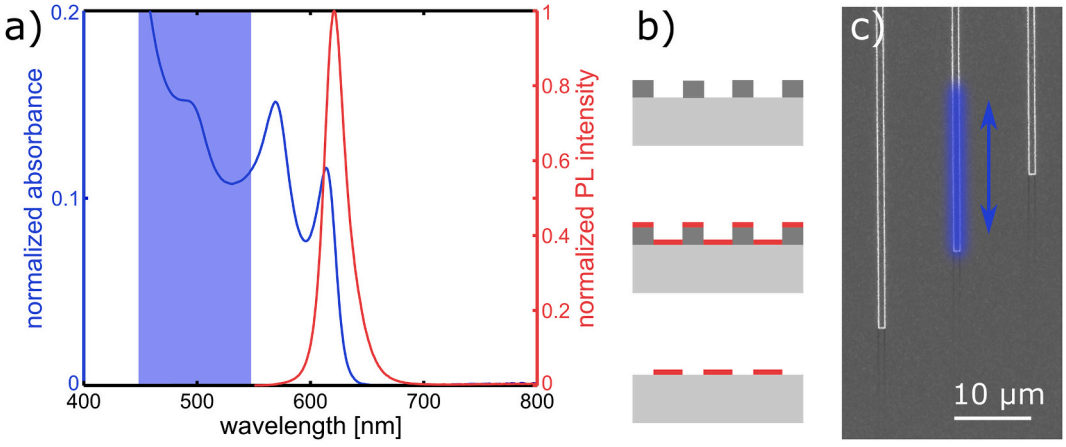

Fig. 1. NPL optical spectra and waveguide geometry. (a) Absorption and PL spectra of the NPLs in hexane solution, the blue box marks the optical excitation range, (b) sketch of the NPL waveguide fabrication by EBL (glass substrate light grey, polymer resist dark grey, NPLs red), (c) SEM image of three exemplary stripes; the laser line focus used for excitation is sketched in blue, the double arrow indicates the line focus shift used for the variable stripe length measurement. (For interpretation of the references to colour in this figure legend, the reader is referred to the web version of this article.)

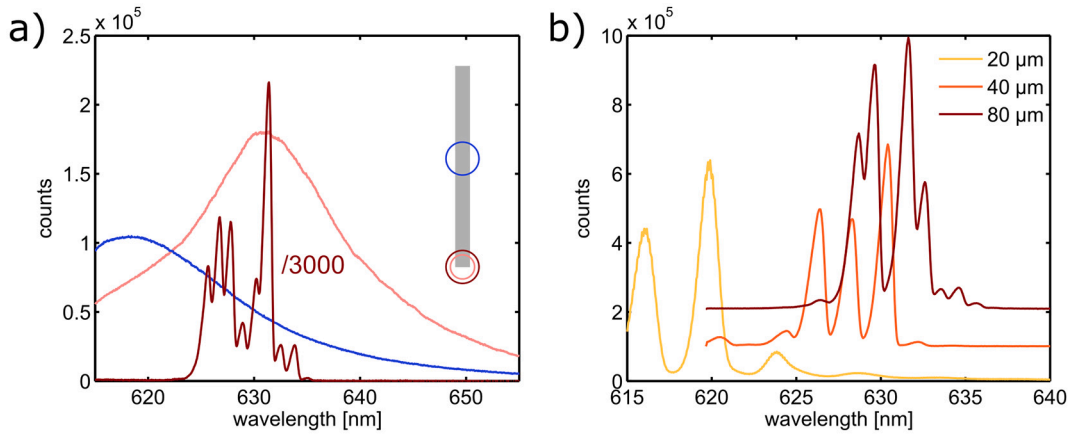

Fig. 2. Nanoplatelet stripe ASE and lasing. (a) Emission spectra from the center of a 70 µm long stripe (PL, blue) and from the stripe end (ASE, light red), both for a pump fluence of 84 µJ/cm^2. The dark red spectrum shows laser emission for a pump fluence of 260 µJ/cm^2. The circles in the inset illustrate where along the stripe waveguide the spectra were acquired. (b) Spectra taken for a pump fluence of of 260 μJ/cm^2 from the end of stripes with lengths of 20, 40 and 80 µm, the spectra are vertically shifted for clarity. (For interpretation of the references to colour in this figure legend, the reader is referred to the web version of this article.)

yield an intensity reflection factor at the stripe end of 5.5 and 3.5% for the stripes 500 nm and 1 µm wide, respectively.

Fig. 3a (left panel) shows the microscope image of a 30 µm long NPL stripe excited with a pump fluence of 84 µJ/cm^2. We observe homogeneous emission all along the stripe, with somewhat brighter stripe ends due to the scattering of guided light. The spatially resolved spectra in the right panel in Fig. 3a confirm the spectrally homogeneous spontaneous emission along the stripe. The spectra at the stripe ends show an additional redshift due to ASE (compare Fig. 2a), which is preferentially emitted into the waveguide mode and scattered at the stripe ends. The slight bend of the signal at the stripe ends is an imaging artifact.

For a pump fluence of 550 μJ/cm^2, which is well above the lasing threshold, light emission from the stripe ends dominates (Fig. 3b), with intensities more than three orders of magnitude larger than below threshold and spectrally narrow peaks (right panel), as expected for lasing. In Fig. 3c the excitation fluence is identical to that in Fig. 3b, however, the outer rim of an iris diaphragm blocks the signals from the stripe ends and the camera exposure time is increased by a factor of 100, as compared to Fig. 3b. We observe laser light that is weakly scattered along the stripe. The ratio of the emission intensities scattered along the stripe (Fig. 3b) and at the stripe ends (Fig. 3c) yields an estimate of the ratio of radiation loss (along the waveguide) to laser output. We integrate the signal along the central 10 µm of the stripe in Fig. 3c, normalize it to the whole stripe length and compare it to the sum of the signals from both ends in Fig. 3b. We find that the radiation loss corresponds to about 15% of the laser output, a value that could possibly be reduced by optimizing the fabrication procedures. This could include optimized spin coating parameters, annealing or even oriented NPL deposition [13]. We note that for a more detailed analysis the angular emission pattern from the light scattered at the stripe end should be considered.

The output light intensities as measured from the stripe terminations versus pump fluence for NPL stripes of different lengths are summarized in Fig. 4a for the 500 nm wide stripes. Clear threshold behavior is observed for increasing pump fluence. The threshold value decreases with increasing structure length, as for shorter structures the gain per length necessary to overcompensate reflection losses (as the main loss contribution) is evidently higher. The threshold is thus highest for the 20 µm long stripe with 130 µJ/cm^2 and lowest for the stripe length of 60 µm length with 50 µJ/cm^2. In Fig. 4b, we plot the corresponding data for the 1 μm wide stripes. Generally, the threshold values are higher here, due to the somewhat lower waveguide mode confinement and end face reflectivity (see the Supporting Information).

Fig. 4c combines the pump fluence dependence of the 40 μm long

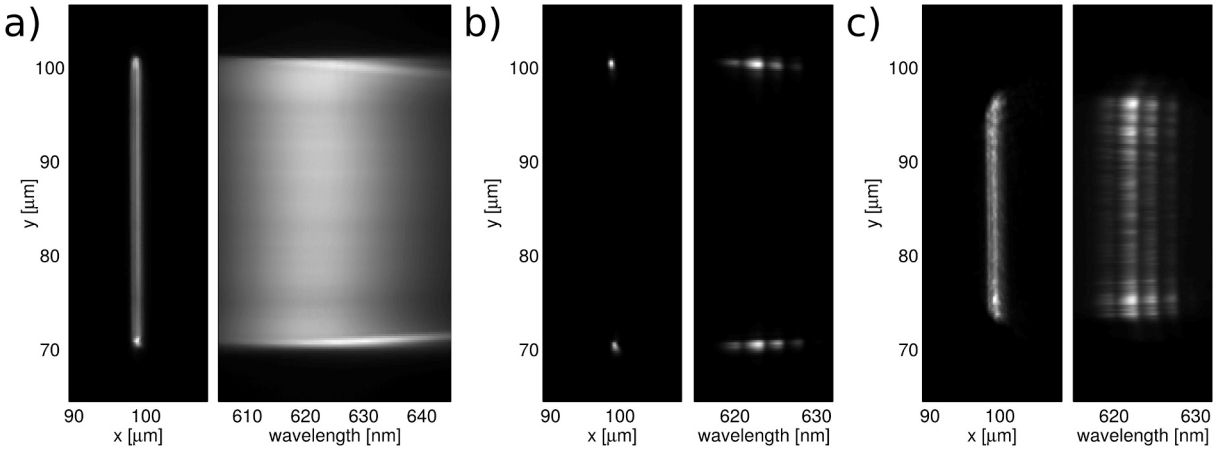

Fig. 3. Images and spatially resolved spectra of the emission of a 30 μm long nanoplatelet stripe, (a) below lasing threshold (pump fluence 84 μJ/cm^2), (b) and (c) above lasing threshold (pump fluence 550 µJ/cm^2). In (c), the emission from the stripe ends has been blocked and the camera exposure time has been increased by a factor 100 to detect scattered light along the stripe. The left-hand panels show the microscopic image of the stripe, in the right-hand panels the horizontal axis is switched to spectral dispersion.

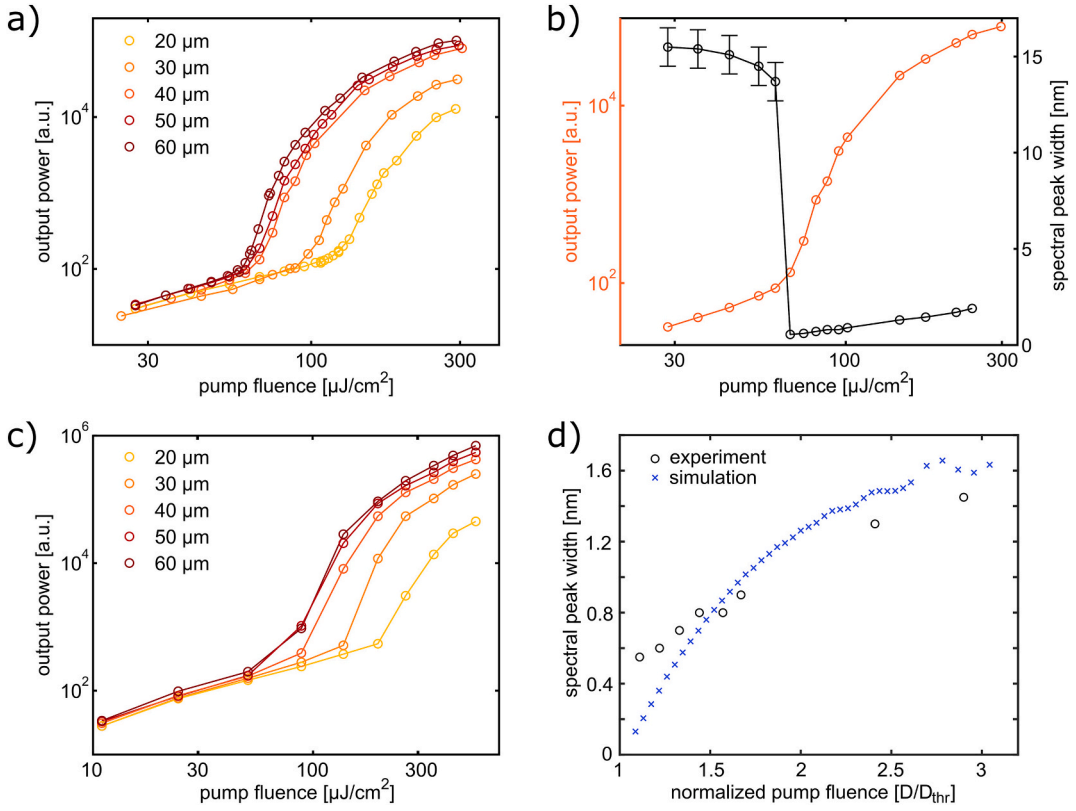

Fig. 4. Emission characteristics of NPL stripes. (a) Output power vs. pump fluence for 500 nm wide stripes of different length from 20 to 60 µm. The emission strongly increases at stripe-length-specific threshold values of the pump fluence. For stronger pumping, emission saturation is observed. (b) Same as (a) for a stripe width of 1 µm. (c) Pump-dependent output power for the 40 µm long stripe (red) and spectral peak fwhm width (black). (d) Measured (circles) and simulated (crosses) spectral peak fwhm for a 40 μm long resonator vs. pump strength, normalized to the threshold pump fluence (experiment) and the threshold pump strength parameter D_{thr} (simulation). (For interpretation of the references to colour in this figure legend, the reader is referred to the web version of this article.)

stripe from Fig. 4a with the corresponding spectral fwhm dependence of the (highest) emission peak. At threshold, the peak width drops from about 15 to below 0.6 nm. Below threshold the error in measuring the spectral width is relatively large, as we have to consider the spontaneous emission background (direct emission) in the ASE signal (scattered from the stripe end) and both signals are of similar magnitude. Above threshold, however, the spontaneous emission contribution is negligible and the error margin becomes smaller than the symbol size in Fig. 4c. Interestingly, above threshold the peak width increases again with increasing pump fluence. We note that this effect is documented in recent literature [26–29], however, without being discussed to the best of our knowledge. We attribute the broadening to pulse shortening with increasing gain, as illustrated by the following simulation.

To capture the essential lasing characteristics of the NPL stripes, we numerically simulate a one-dimensional model with varying length L. We solve the time-dependent Maxwell-Bloch equations [30] for different pump strengths D that we keep constant during the time interval corresponding to the duration of one pump pulse, i.e., 6 ps. Our input parameters are the lasing transition frequency $\nu_0 = 4.76 \times 10^{14}$ Hz, an estimated propagation loss along the stripe $d = 100\ cm^{-1}$, the relaxation times $T1 \equiv 1/\gamma_{\parallel} = 2$ ns and $T2 \equiv 1/\gamma_{\perp} = 7.8$ fs and an assumed refractive index of 1.5. In the Maxwell-Bloch equations, the parameters $\gamma_{\parallel}$ and $\gamma_{\perp}$ describe the decay constants of the population inversion and of the polarization, respectively. Therefore, the relaxation time T1 corresponds to the fluorescence lifetime, whereas T2 represents the mean dephasing time of the gain medium (for further details see the Supporting Information.)

Although this 1D model is rather simple, we find a convincing agreement between measurements and simulated results. Similar as in the experiments, our simulations show that the spectral peak width of the laser emission above threshold increases with increasing pump strength, as depicted in Fig. 4d for the resonator length of 40 µm. We note that the pump strength parameter D that enters our numerical simulations is not identical to the pump fluence from the experiment, but rather represents the externally imposed inversion. Assuming a linear correlation between these two quantities, we find that the simulation matches rather well with the experimental data, keeping the simplicity of our approach in mind. To address remaining deviations, a more comprehensive simulation of the laser dynamics would be required. In particular, we expect that to be quantitatively accurate, such a model needs to include the effects of temperature-related broadening due to heating, noise due to mechanisms like spontaneous emission, and potential experimental imperfections as fabrication errors.

Fig. 5a shows the simulated spectra of a 20 µm long structure for two different pump strengths of 1.8 (blue) and 4.5 (red) times the threshold pump strength D_{thr}. Besides the pump strength dependence of the laser line width, the overall shape corresponds well to the experimental observation in Fig. 2b. We further explore the temporal effects in Fig. 5b for stripe lengths of 20, 30 and 40 μm. We find that the laser pulse is indeed shortened above threshold with increasing pump strength. For example, for the 40 μm long structure, the pulse duration is 6 ps just above threshold and drops to 2 ps for a value about twice D_{thr}. For the 20 μm long structure pulse lengths below 1 ps are observed. We attribute the effect of pulse shortening with increasing pump power to the fact that a higher population inversion leads to an increasingly faster buildup of the lasing mode and thus to a shortening of the leading edge of the pulse. Since also the resulting field strength in the cavity grows with increasing pump power, the inversion is depleted more quickly such that the trailing edge is shortened as well, where the cavity properties (i.e.,

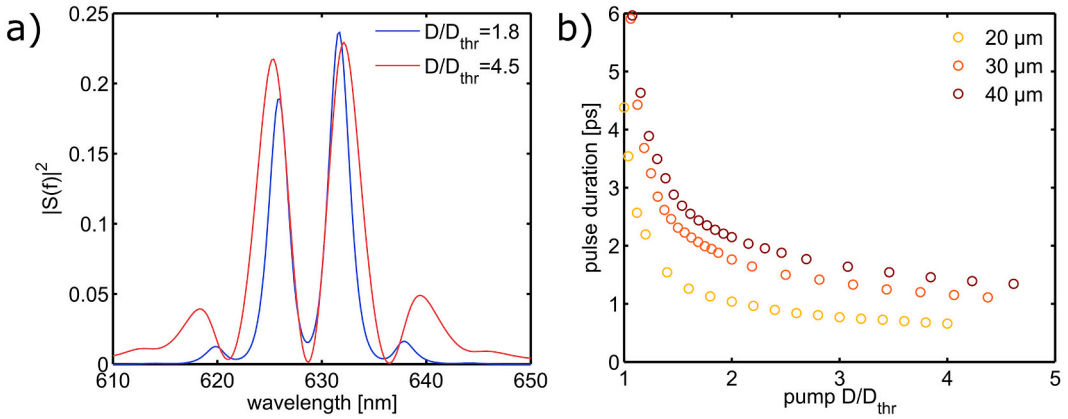

Fig. 5. (a) Simulated spectra for the one-dimensional NPL model with 20μm length at a pump strength normalized to the threshold pump strength D_{thr} of 1.8 (blue) and 4.5 (red). (b) Simulated pulse duration as a function of normalized pump strength for 20, 30 and 40μm resonator length. (For interpretation of the references to colour in this figure legend, the reader is referred to the web version of this article.)

length, loss, and outcoupling) determine a lower bound for the pulse duration. These effects are clearly needed to be considered with care for the optimization and application of lasers which combine small size with high gain.

The modal gain of the NPL stripes was deduced with the VSL method, [31,32] applied to the stripe waveguides for pump intensities below the laser threshold. For this purpose, the reflection from one end of a 1 µm wide NPL stripe was eliminated by adiabatically expanding the stripe into an extended film, see Fig. 6a. Different stripe lengths were then overlayed with the laser line focus in increments of 5 µm with a piezoactuator stage. The pump fluence was set to 250 µJ/cm^2.

The measured light intensities scattered from the free stripe end are plotted in Fig. 6b as a function of the stripe length that was excited by the laser line focus. The data (circles) are fitted exponentially (curve) by taking into account a constant background c_0 from spontaneous emission around the stripe end. Further, we consider a background c_1 from spontaneous emission into the waveguide mode that depends on the excited stripe length x, so that we describe the total intensity as $I_x = (I_0/g)(e^{gx} - 1) + c_0 + c_1 x$, with gain g. We note that with the stripe length range considered here we are well within the validity range of the VSL method to respect to stripe-length-independent gain [15].

From the combined data of five nominally identical stripes we deduce a gain value of 1630 ± 170 cm^{-1}. This value agrees well with the simulated stripe end-face reflectivity. For an end face reflectivity of 4%, the ratio of gain-induced signal increase along the stripe to end face reflectivity has to be 25. For the shortest resonator length of 20 µm, this corresponds to a required gain of about 1600 cm^{-1}. Furthermore, as the gain is increasing with the pump intensity, the quite moderate pump level used here leaves space for further improvement.

4. Conclusion

In conclusion, we have demonstrated a remarkably high gain value of about 1630 cm^{-1} for CdSe/CdS NPLs. Lasing was achieved with a simple monolithic stripe waveguide structure that (although built by EBL here) could be fabricated by scalable techniques as imprinting. It has to be emphasized that lasing relying on the low reflectivity of the waveguide end faces was only possible due to the high gain involved. This leads however ample room for improvement with, e.g., Bragg mirror geometries for efficient feedback. All-NPL waveguides including Bragg mirrors have been recently reported [20]. We have looked into the temporal emission dynamics and evidenced pulse shortening for increasing pump levels above laser threshold. Building on these results, further steps in the application of NPLs for micro- and nanophotonics can be envisioned.

5. Methods

5.1. Nanoplatelet synthesis

21 mg of purified CdSe NPLs in 5 mL hexane were mixed with 5 mL of *N*-methylformamide (MFA) and 50 µL of 40–48% $(NH_4)_2S$ aqueous solution. After complete phase transfer within 3–5 min, the NPLs in MFA were rinsed three times with 5 mL of fresh hexane and precipitated with

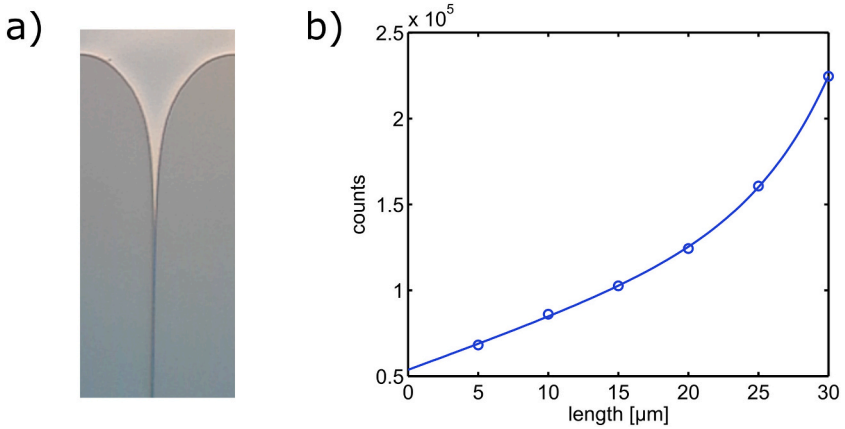

Fig. 6. Gain measurement with the VSL method. (a) Optical microscope image of a NPL stripe tapered into a NPL film to eliminate reflection. (b) Measured emission intensity dependent on the stripe length excited by the laser line focus (circles), the curve is a fit of I_x (see text) to the data.

5 mL acetonitrile (ACN) and 8 mL toluene. The precipitated NPLs were redissolved in 2 mL MFA and mixed with 2.5 mL of a 0.2 M solution of $Cd(Ac)_2$ in MFA. After 1 min, the NPLs were precipitated with 8 mL toluene. The pellet was redissolved in 2 mL MFA and mixed with 2.5 mL of a $(NH_4)_2S$ solution in MFA (20 μL $(NH_4)_2S$ in 1 mL MFA). After one minute, the NPLs were precipitated with 8 mL toluene. The last two steps were repeated two more times for the Cd and one more time for the S layers to complete three monolayers of CdS. The obtained pellet (Cd-terminated CdSe/CdS NPLs) was redissolved in 2 mL hexane with 250 μL oleylamine (70%). An excess of oleylamine was removed by one more precipitation step with 1.8 mL ethanol and redissolution in 3 mL hexane. The final solution was filtered through a 0.2 μm polytetrafluoroethylene filter.

5.2. Electron beam lithography

For the lithographic waveguide fabrication, we used the beam of a scanning electron microscope to expose the waveguide geometry in a 600 nm thick poly(methylmetacrylate) (PMMA) resist film on a cover slide glass substrate. An additional 100 nm thick layer of a conductive polymer (Allresist, AR-PC 5090) provides electric conductivity to prevent charging. After exposure, removal of the water-soluble conductive polymer layer and chemical development of the PMMA mask, we deposited NPLs by spin-coating a 2 μMol solution in hexane at 3000 rpm. A final lift-off step of the PMMA film concludes the fabrication. A scanning electron image of the resulting waveguide surface is depicted in the Supporting Information.

Author contributions

M.B. sample preparation, experiments, data analyis, image preparation; D.N.D. and M.V.K. nanoplatelet synthesis; K.P. and S.R. numerical simulations; A.G. ASE measurements; H.D., A.H. and J.R.K. conceptualization and supervision, J.R.K., M.B., K.P. and D.N.D. writing of the manuscript; all authors proofread the final manuscript.

Declaration of Competing Interest

The authors declare the following financial interests/personal relationships which may be considered as potential competing interests:

Joachim R Krenn reports financial support was provided by Austrian Science Fund.

Data availability

Data will be made available on request.

Acknowledgements

This work was supported by FWF SFB NextLite (F4905-N23), NAWI Graz, and the Graz Centre for Electron Microscopy (ZFE). K.P. thanks Stefan Burkhardt for providing his laser code and we acknowledge helpful discussions with Matthias Liertzer.

Appendix A. Supplementary data

Supplementary data to this article can be found online at https://doi.org/10.1016/j.mne.2022.100167.

References

[1] V.I. Klimov, A.A. Mikhailovsky, S. Xu, A. Malko, J.A. Hollingsworth, C. A. Leatherdale, H.J. Eisler, M.G. Bawendi, Optical gain and stimulated emission in nanocrystal quantum dots, Science 290 (2000) 314–317. URL: http://science.sciencemag.org/content/290/5490/314.short.

[2] F. Di Stasio, A. Polovitsyn, I. Angeloni, I. Moreels, R. Krahne, Broadband amplified spontaneous emission and random lasing from Wurtzite CdSe/CdS "Giant-Shell" nanocrystals, ACS Photon. 3 (2016) 2083–2088, https://doi.org/10.1021/acsphotonics.6b00452.

[3] F. Garca-Santamara, Y. Chen, J. Vela, R.D. Schaller, J.A. Hollingsworth, V. I. Klimov, Suppressed auger recombination in "Giant" nanocrystals boosts optical gain performance, Nano Lett. 9 (2009) 3482–3488, https://doi.org/10.1021/nl901681d.

[4] C. Gollner, J. Ziegler, L. Protesescu, D.N. Dirin, R.T. Lechner, G. Fritz-Popovski, M. Sytnyk, S. Yakunin, S. Rotter, A.A. Yousefi Amin, C. Vidal, C. Hrelescu, T. A. Klar, M.V. Kovalenko, W. Heiss, Random lasing with systematic threshold behavior in films of CdSe/CdS Core/thick-Shell colloidal quantum dots, ACS Nano 9 (2015) 9792–9801, https://doi.org/10.1021/acsnano.5b02739.

[5] J. Lim, Y.S. Park, V.I. Klimov, Optical gain in colloidal quantum dots achieved with direct-current electrical pumping, Nat. Mater. 17 (2018) 42–50, https://doi.org/10.1038/NMAT5011.

[6] V.I. Klimov, S.A. Ivanov, J. Nanda, M. Achermann, I. Bezel, J.A. McGuire, A. Piryatinski, Single-exciton optical gain in semiconductor nanocrystals, Nature 447 (2007) 441–446, https://doi.org/10.1038/nature05839.

[7] M. Pelton, Carrier dynamics, optical gain, and lasing with colloidal quantum wells, J. Phys. Chem. C 122 (2018) 10659–10674, https://doi.org/10.1021/acs.jpcc.7b12629.

[8] C. She, I. Fedin, D.S. Dolzhnikov, A. Demortière, R.D. Schaller, M. Pelton, D. V. Talapin, Low-threshold stimulated emission using colloidal quantum wells, Nano Lett. 14 (2014) 2772–2777, https://doi.org/10.1021/nl500775p.

[9] M.D. Tessier, C. Javaux, I. Maksimovic, V. Loriette, B. Dubertret, Spectroscopy of single CdSe nanoplatelets, ACS Nano 6 (2012) 6751–6758, https://doi.org/10.1021/nn3014855.

[10] Y. Altintas, K. Gungor, Y. Gao, M. Sak, U. Quliyeva, G. Bappi, E. Mutlugun, E. H. Sargent, H.V. Demir, Giant alloyed hot injection shells enable ultralow optical gain threshold in colloidal quantum wells, ACS Nano 13 (2019) 10662–10670, https://doi.org/10.1021/acsnano.9b04967.

[11] Y. Kelestemur, Y. Shynkarenko, M. Anni, S. Yakunin, M.L. De Giorgi, M. V. Kovalenko, Colloidal cdse quantum wells with graded shell composition for low-threshold amplified spontaneous emission and highly efficient electroluminescence, ACS Nano 13 (2019) 13899–13909, https://doi.org/10.1021/acsnano.9b05313.

[12] J.Q. Grim, S. Christodoulou, F. Di Stasio, R. Krahne, R. Cingolani, L. Manna, I. Moreels, Continuous-wave biexciton lasing at room temperature using solution-processed quantum wells, Nat. Nanotechnol. 9 (2014) 891–895, https://doi.org/10.1038/NNANO.2014.213.

[13] O. Erdem, S. Foroutan, N. Gheshlaghi, B. Guzelturk, Y. Altintas, H.V. Demir, Thickness-tunable self-assembled colloidal nanoplatelet films enable ultrathin optical gain media, Nano Lett. 20 (2020) 6459–6465, https://doi.org/10.1021/acs.nanolett.0c02153.

[14] B. Guzelturk, Y. Kelestemur, M. Olutas, S. Delikanli, H.V. Demir, Amplified spontaneous emission and lasing in colloidal Nanoplatelets, ACS Nano 8 (2014) 6599–6605, https://doi.org/10.1021/nn5022296.

[15] B. Guzelturk, M. Pelton, M. Olutas, H.V. Demir, Giant modal gain coefficients in colloidal II-VI Nanoplatelets, Nano Lett. 19 (2019) 277–282, https://doi.org/10.1021/acs.nanolett.8b03891.

[16] C. She, I. Fedin, D.S. Dolzhnikov, P.D. Dahlberg, G.S. Engel, R.D. Schaller, D. V. Talapin, Red, yellow, green, and blue amplified spontaneous emission and lasing using colloidal CdSe nanoplatelets, ACS Nano 9 (2015) 9475–9485, https://doi.org/10.1021/acsnano.5b02509.

[17] Z. Yang, M. Pelton, I. Fedin, D.V. Talapin, E. Waks, A room temperature continuous-wave nanolaser using colloidal quantum wells, Nat. Commun. 8 (2017) 143, https://doi.org/10.1038/s41467-017-00198-z.

[18] M. Li, M. Zhi, H. Zhu, W.Y. Wu, Q.H. Xu, M.H. Jhon, Y. Chan, Ultralow-threshold multiphoton-pumped lasing from colloidal nanoplatelets in solution, Nat. Commun. 6 (2015) 8513, https://doi.org/10.1038/ncomms9513.

[19] P. Geiregat, D. Van Thourhout, Z. Hens, A bright future for colloidal quantum dot lasers, NPG Asia Mat. 11 (2019) 41, https://doi.org/10.1038/s41427-019-0141-y.

[20] N. Gheshlaghi, S. Foroutan-Barenji, O. Erdem, Y. Altintas, F. Shabani, M. H. Humayun, H.V. Demir, Self-resonant microlasers of colloidal quantum wells constructed by direct deep patterning, Nano Lett. 21 (2021) 4598–4605, https://doi.org/10.1021/acs.nanolett.1c00464.

[21] S. Ithurria, B. Dubertret, Quasi 2D colloidal CdSe platelets with thicknesses controlled at the atomic level, J. Am. Chem. Soc. 130 (2008) 16504–16505, https://doi.org/10.1021/ja807724e.

[22] L. Piveteau, T.C. Ong, B.J. Walder, D.N. Dirin, D. Moscheni, B. Schneider, J. Bär, L. Protesescu, N. Masciocchi, A. Guagliardi, L. Emsley, C. Copéret, M.V. Kovalenko, Resolving the core and the surface of CdSe quantum dots and nanoplatelets using dynamic nuclear polarization enhanced PASS–PIETA NMR spectroscopy, ACS Cent. Sci. 4 (2018) 1113–1125, https://doi.org/10.1021/acscentsci.8b00196.

[23] M. Olutas, B. Guzelturk, Y. Kelestemur, A. Yeltik, S. Delikanli, H.V. Demir, Lateral size-dependent spontaneous and stimulated emission properties in colloidal CdSe nanoplatelets, ACS Nano 9 (2015) 5041–5050, https://doi.org/10.1021/acsnano.5b01927.

[24] V.I. Klimov, Spectral and dynamical properties of multiexcitons in semiconductor nanocrystals, Annu. Rev. Phys. Chem. 58 (2007) 635–673, https://doi.org/10.1146/annurev.physchem.58.032806.104537.

[25] V.I. Klimov, A.A. Mikhailovsky, D.W. McBranch, C.A. Leatherdale, M.G. Bawendi, Quantization of multiparticle auger rates in semiconductor quantum dots, Science 287 (2000) 1011–1013. URL: http://science.sciencemag.org/content/287/5455/1011 https://doi.org/10.1126/science.287.5455.1011.

[26] J. Ho, J. Tatebayashi, S. Sergent, C.F. Fong, Y. Ota, S. Iwamoto, Y. Arakawa, A nanowire-based plasmonic quantum dot laser, Nano Lett. 16 (2016) 2845–2850, https://doi.org/10.1021/acs.nanolett.6b00706.
[27] S.J.P. Kress, J. Cui, P. Rohner, D.K. Kim, F.V. Antolinez, K.A. Zaininger, S. V. Jayanti, P. Richner, K.M. McPeak, D. Poulikakos, D.J. Norris, A customizable class of colloidal-quantum-dot spasers and plasmonic amplifiers, Sci. Adv. 3 (2017) e1700688. URL: http://advances.sciencemag.org/content/3/9/e1700688 https://doi.org/10.1126/sciadv.1700688.
[28] H.T. Rekola, T.K. Hakala, P. Törmä, One-dimensional plasmonic nanoparticle chain lasers, ACS Photon. 5 (2018) 1822–1826, https://doi.org/10.1021/acsphotonics.8b00001.
[29] K. Roh, L. Zhao, B.P. Rand, Tuning laser threshold within the large optical gain bandwidth of halide perovskite thin films, ACS Photon. 8 (2021) 2548–2554, doi:0000.
[30] S. Burkhardt, M. Liertzer, D.O. Krimer, S. Rotter, Steady-state ab initio laser theory for fully or nearly degenerate cavity modes, Phys. Rev. A 92 (2015), 013847, https://doi.org/10.1103/PhysRevA.92.013847.
[31] L. Dal Negro, P. Bettotti, M. Cazzanelli, D. Pacifici, L. Pavesi, Applicability conditions and experimental analysis of the variable stripe length method for gain measurements, Opt. Commun. 229 (2004) 337–348, https://doi.org/10.1016/j.optcom.2003.10.051.
[32] K.L. Shaklee, R.F. Leheny, Direct determination of optical gain in semiconductor crystals, Appl. Phys. Lett. 18 (1971) 475–477, https://doi.org/10.1063/1.1653501.